RAA 2018 Vol. **18** No. **3**, 36(8pp) doi: 10.1088/1674–4527/18/3/36

http://www.raa-journal.org *http://iopscience.iop.org/raa*

Research in Astronomy and Astrophysics

Accreting CO material onto ONe white dwarfs towards accretion-induced collapse

Cheng-Yuan Wu and Bo Wang

Yunnan Observatories, Chinese Academy of Sciences, Kunming 650216, China; *wcy@ynao.ac.cn; wangbo@ynao.ac.cn*
Key Laboratory for the Structure and Evolution of Celestial Objects, Chinese Academy of Sciences, Kunming 650216, China
University of Chinese Academy of Sciences, Beijing 100049, China
Center for Astronomical Mega-Science, Chinese Academy of Sciences, Beijing 100012, China

Received 2017 December 4; accepted 2018 January 28

Abstract The final outcomes of accreting ONe white dwarfs (ONe WDs) have been studied for several decades, but there are still some issues that are not resolved. Recently, some studies suggested that the deflagration of oxygen would occur for accreting ONe WDs with Chandrasekhar masses. In this paper, we aim to investigate whether ONe WDs can experience accretion-induced collapse (AIC) or explosions when their masses approach the Chandrasekhar limit. Employing the stellar evolution code `Modules for Experiments in Stellar Astrophysics` (`MESA`), we simulate the long-term evolution of ONe WDs with accreting CO material. The ONe WDs undergo weak multicycle carbon flashes during the mass-accretion process, leading to mass increase of the WDs. We found that different initial WD masses and mass-accretion rates influence the evolution of central density and temperature. However, the central temperature cannot reach the explosive oxygen ignition temperature due to neutrino cooling. This work implies that the final outcome of accreting ONe WDs is electron-capture induced collapse rather than thermonuclear explosion.

Key words: stars: evolution — binaries: close — supernovae: general — white dwarfs

1 INTRODUCTION

Carbon-oxygen white dwarfs (CO WDs) in binaries are expected to form type Ia supernovae (SNe Ia) when they grow in mass close to the Chandrasekar limit ($M_{\rm Ch}$; e.g., Hachisu et al. 1996; Li & van den Heuvel 1997; Han & Podsiadlowski 2004; Wang et al. 2009, 2013; Wu et al. 2016; Wang 2018). However, the final outcomes may be changed if the primary stars are oxygen-neon white dwarfs (ONe WDs). An electron-capture induced collapse would occur in an accreting ONe WD when its mass increases to $M_{\rm Ch}$, resulting in the formation of a neutron star (NS) (e.g., Miyaji et al. 1980; Nomoto & Kondo 1991). This process is referred to as accretion-induced collapse (AIC), and is related to the formation of some important objects, such as low-mass binary pulsars, millisecond pulsars (MSPs) and magnetars (e.g., Bailyn & Grindlay 1990; Bhattacharya & van den Heuvel 1991; Usov 1992; Dar et al. 1992; Podsiadlowski et al. 2002; Tauris et al. 2013). According to a detailed population synthesis study, Hurley et al. (2010) suggested that the birthrates of binary MSPs from the AIC scenario are comparable to those from core collapse supernovae, which means that the AIC scenario plays an important role in forming binary MSPs. AIC may also be related to r-process nucleosynthesis and the formation of ultrahigh-energy cosmic rays like gamma-ray bursts (e.g., Hartmann et al. 1985; Fryer et al. 1999; Qian & Wasserburg 2007; Metzger et al. 2008; Piro & Kollmeier 2016; Lyutikov & Toonen 2017). In observations, it is useful in understanding binary evolution and the forma-

tion of NSs in globular clusters by identifying electromagnetic signatures of AIC and constraining its birthrate (e.g., Moriya 2016). Moreover, AIC may also be a potential source of strong gravitational wave emission (e.g., Abdikamalov et al. 2010).

There are two fundamental progenitor models for AIC. (1) The first one is the single-degenerate model, in which an ONe WD accretes H/He-rich material from its non-degenerate companion via Roche-lobe overflow. During the mass-transfer process, the accumulated material is transformed into heavier elements due to multi-shell burning. Eventually, AIC may occur if an ONe WD increases its mass to $M_{\rm Ch}$ (e.g., Nomoto & Kondo 1991; Langer et al. 2000; Tauris et al. 2013; Brooks et al. 2017). Additionally, CO WD + He star systems may also contribute to the formation of NSs through AIC when off-center carbon ignition occurs on the surface of the WD (e.g., Brooks et al. 2016; Wang et al. 2017). (2) The second one is the double-degenerate (DD) model, in which two WDs in binaries are brought together due to gravitational wave radiation. The WD will grow in mass via mass-transfer from its donor. Finally, the primary WD may collapse into an NS if the combined mass exceeds $M_{\rm Ch}$ (e.g., Nomoto & Iben 1985). So far, three merger models have been widely discussed, i.e., the slow merger model, the fast merger model and the composite model. In the slow merger model, the mass ratio of two WDs should be less than $2/3$, and stable mass transfer can occur. The mass donor will be tidally disrupted and form an accretion disc around the primary WD, and the accretion rate from the disc is around the Eddington rate (e.g., Saio & Jeffery 2000, 2002). In the fast merger model, the merger process is dynamically unstable and may last for a few minutes. All material in the companion will be transferred onto the surface of the primary and forms a corona (e.g., Benz et al. 1990; Schwab et al. 2016). In the composite model, part of the material forms a corona and the remaining material forms a Keplerian disc, in which both the fast and slow merger processes are included (e.g., Yoon et al. 2007; Zhang et al. 2014). Generally, WD binaries in the DD model could be ONe WD + CO/ONe WD systems (e.g., Schwab et al. 2015; Lyutikov & Toonen 2017). Some studies also indicate that CO WD + CO WD systems could be progenitors of AIC (e.g., Saio & Nomoto 2004; Schwab et al. 2016).

However, the final fate of an ONe WD with $M_{\rm Ch}$ has been questioned by some recent studies (e.g., Marquardt et al. 2015; Jones et al. 2016). Since the WD contains nuclear fuel inside (e.g., ^{16}O, ^{20}Ne and maybe ^{12}C for a less massive WD), and may experience electron capture as well as subsequent exothermic reactions of γ-decay, the ONe WD can undergo explosive oxygen or neon burning. A population of such WDs would then produce a subpopulation of SNe Ia when their mass approaches $M_{\rm Ch}$. Note that whether an ONe WD goes through collapse or explosion is determined by the competition between electron capture and nuclear burning; the final fate may also be dependent on different conditions of deflagration wave propagation and criteria of explosive nucleosynthesis (e.g., Nomoto & Kondo 1991; Jones et al. 2016). Therefore, there are still some uncertainties in the final outcomes of ONe WDs with $M_{\rm Ch}$, the study of which is useful in understanding the formation of electron-capture supernovae and SNe Ia.

In this paper, we examine the long-term evolution of ONe WDs when accreting CO material, and investigate the final fate of ONe WDs, in which we will consider different initial WD masses ($M^{\rm i}_{\rm WD}$) and mass-accretion rates ($\dot{M}_{\rm acc}$). In Section 2, we introduce our basic assumptions and methods for numerical calculations. The results from our simulations are provided in Section 3. Finally, we present discussion and conclusions in Section 4.

2 METHODS

We employ the stellar evolution code named `Modules for Experiments in Stellar Astrophysics` (`MESA`; version 7624) (see Paxton et al. 2011, 2013, 2015) to simulate the long-term evolution of ONe WDs when accreting CO material. Our simulations can be divided into two steps.

Firstly, we use the module `make_low_mass_with_uniform_composition` to construct ONe WDs with a uniform elemental abundance distribution, in which the mass fractions are 50% ^{16}O, 45% ^{20}Ne and 5% ^{24}Mg. These elemental abundances are similar to those of some previous studies (e.g., Takahashi et al. 2013; Schwab et al. 2015). We cool down the ONe cores until their luminosity decreases to $10^2\ L_{\odot}$, which we use as our initial WD models.

Secondly, we utilize the module `wd_aic` to simulate the mass-accretion processes of the ONe WDs. The nuclear reaction network adopted in our simulations includes 23 isotopes needed for carbon, oxygen and neon burning (e.g., ^{12}C, ^{16}O, ^{20}Ne, ^{24}Mg), which are coupled by more than 100 reactions. We consider the electron-

capture reactions for ^{24}Mg and ^{20}Ne (i.e., $^{24}\mathrm{Mg} \rightarrow {}^{24}\mathrm{Na} \rightarrow {}^{24}\mathrm{Ne}$; $^{20}\mathrm{Ne} \rightarrow {}^{20}\mathrm{F} \rightarrow {}^{20}\mathrm{O}$) and β-decay reactions (the reverse reactions for electron captures). We also consider the ion Coulomb corrections and the electron Coulomb corrections in our simulations (e.g., Potekhin et al. 2009; Itoh et al. 2002). We use the temperature as the criterion to examine whether AIC can occur. If the central temperature of the WD exceeds a critical value for explosive neon or oxygen burning (e.g., $\log T_{\rm c} \sim 9.6$) at the final stage of evolution, the core will experience a thermonuclear supernova explosion, otherwise, the outcome is treated as a collapse.

We adopt constant accretion rates to simulate the mass-accretion process, in which the accreted CO material consists of 50% ^{12}C and 50% ^{16}O. The range of accretion rates is $1.0 \times 10^{-9} \leq \dot{M}_{\rm acc} \leq 2.0 \times 10^{-5}\,M_{\odot}\,{\rm yr}^{-1}$, which could represent the thick disc model or slow merger model (e.g., Saio & Jeffery 2000, 2002; Zhang & Jeffery 2012). In this model, if the mass ratio of two WDs is sufficiently large, the less massive WD in a binary will be dynamically disrupted when it fills its Roche lobe and forms a pressure or centrifugalization supported disc surrounding the more massive WD. The mass-transfer rate from the pressure supported disc to the primary WD may be close to the Eddington accretion rate. However, the accretion rate could be less than $5.0 \times 10^{-6}\,M_{\odot}\,{\rm yr}^{-1}$ for the centrifugalization supported disc and the disc may last for $10^4 - 10^6$ yr (e.g., Mochkovitch & Livio 1990; Yoon et al. 2007; Zhang & Jeffery 2012; Zhang et al. 2014). This mass-loss mechanism is included in our simulations. Here, we assume that a super-Eddington wind will be triggered and blows away part of the material from the envelope when the surface luminosity exceeds the Eddington luminosity (see also Denissenkov et al. 2013; Wang et al. 2015; Wu et al. 2017).

3 NUMERICAL RESULTS

3.1 An Example of AIC

In Figures 1–5, we present an example of the long-term evolution of an accreting ONe WD, in which $M^{\rm i}_{\rm WD} = 1.2\,M_{\odot}$ and $\dot{M}_{\rm acc} = 1.0 \times 10^{-5}\,M_{\odot}\,{\rm yr}^{-1}$.

Figure 1 shows the luminosity, radius and mass of the WD as functions of time during the mass accumulation process. The CO material piles up on the surface of the WD during the mass-accretion process, and the CO envelope is heated up by the release of gravitational potential energy, leading to carbon ignition. The flame in the shell transforms the carbon into neon and magnesium, and these heavier elements are mixed into the ONe core by convection, resulting in mass increase of the WD. A super-Eddington wind is triggered when the luminosity exceeds the Eddington luminosity that can blow away part of the material. However, the carbon flashes in our simulations are too weak to blow away too much material, resulting in mass increase of the WD; the radius of the WD decreases gradually since the ONe core becomes more massive. Meanwhile, the luminosity changes by about an order of magnitude due to unstable carbon shell burning and fluctuates frequently as the surface temperature increases.

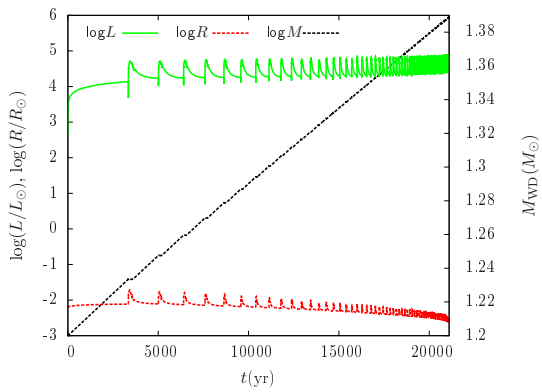

Fig. 1 Long-term evolution of a $1.2\,M_{\odot}$ accreting WD that undergoes weak carbon flashes. The *green solid line*, *red dashed line* and *black dashed line* represent the luminosity, WD radius and WD mass as functions of time during the accretion process, respectively.

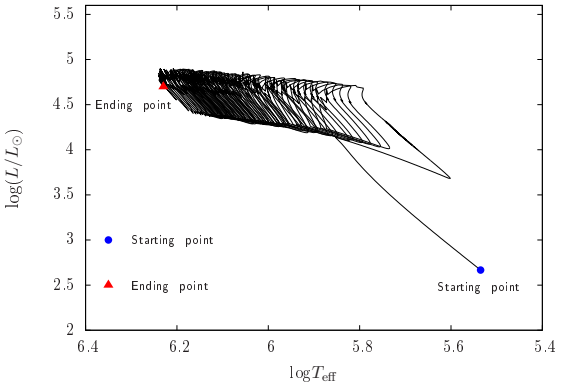

Fig. 2 The Hertzsprung-Russell diagram of a $1.2\,M_{\odot}$ ONe WD during weak carbon flashes. The *blue filled circle* and *red filled triangle* represent the starting and ending points, respectively.

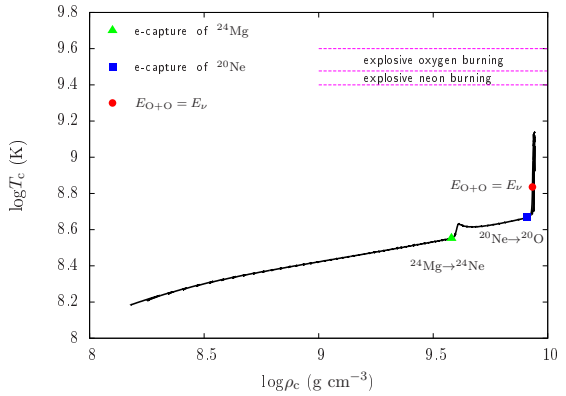

Fig. 3 Central density-temperature profile for the evolution of a $1.2\,M_\odot$ ONe WD during mass accumulation. The *green triangle* and *blue square* are the starting points of electron-capture reactions for ^{24}Mg and ^{20}Ne, respectively. The *red circle* is the point where the nuclear reaction energy generation from oxygen burning equals the neutrino losses. The *pink dashed lines* show the critical temperature range for explosive neon and oxygen burning.

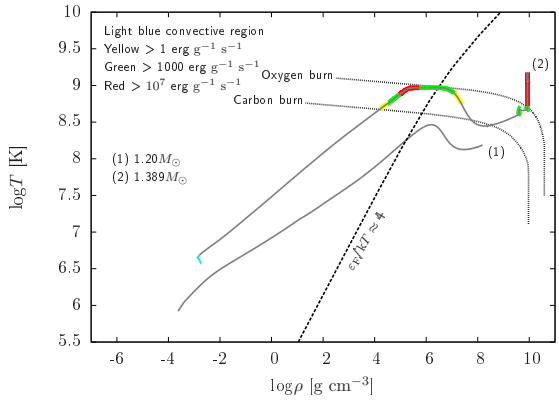

Fig. 4 Density-temperature profile of the initial and final ONe WD. The initial profile is represented by line (*1*), whereas the final profile is represented by line (*2*).

Figure 2 presents the Hertzsprung-Russell diagram of the accreting WD. The CO material is accumulated onto the surface of the WD at the onset of the accretion process, resulting in the increase of luminosity (L) and effective temperature ($T_{\rm eff}$) via the release of gravitational potential energy. The carbon in the shell is ignited after L exceeds $10^4 L_\odot$, resulting in the expansion of the envelope and the decrease of L and $T_{\rm eff}$. However, the formed convection zone effectively transfers heat from the inside out, and the envelope of the WD stops expanding during this stage, leading to an increase of L and $T_{\rm eff}$. The WD rapidly enters the cooling phase after

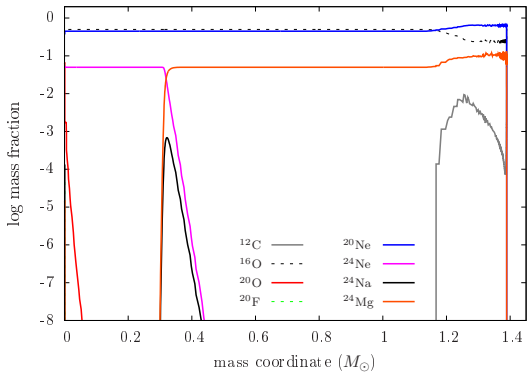

Fig. 5 Elemental abundance distribution profile of the ONe WD at the final moment.

it experiences the super-Eddington wind stage. The WD undergoes more than 60 carbon flashes during the evolution, and AIC finally occurs when its mass approaches $1.39 M_\odot$.

Figure 3 presents the central density-temperature profile of the ONe WD during the evolution process. The WD becomes more massive due to multiple carbon shell flashes, leading to an increase of central density ($\rho_{\rm c}$) and temperature ($T_{\rm c}$). After $\rho_{\rm c}$ approaches the point where the electron-capture timescale of ^{24}Mg equals the core compression timescale (i.e., $t_{\rm compress} \approx 5 \times 10^4\,{\rm yr}\,(\frac{\rho_{\rm c}}{10^9\,{\rm g\,cm^{-3}}})^{-0.55}\,(\frac{\dot{M}}{10^{-6}\,M_\odot\,{\rm yr^{-1}}})^{-1}$; see Schwab et al. 2015), $T_{\rm c}$ increases owing to the exothermic reactions of electron capture until the exhaustion of central ^{24}Mg. A similar phenomenon of rapid increase of $T_{\rm c}$ occurs when $\rho_{\rm c}$ approaches the blue point, where the electron-capture reaction of ^{20}Ne is triggered. Since the mass fraction of ^{20}Ne is 45%, the electron-capture process of ^{20}Ne can last for a long time, resulting in the occurrence of ^{16}O+^{16}O nuclear reactions. After the oxygen burning is ignited, $T_{\rm c}$ obviously increases owing to an exothermic process through electron capture and oxygen burning. However, the neutrino energy loss rate $\varepsilon_\nu \propto T^9$ when the temperature exceeds 10^9K. Subsequently, energy release of the nuclear reactions cannot balance energy loss at the high temperature, leading to a decrease of $T_{\rm c}$. The highest $T_{\rm c}$ of the WD in our simulations is 1.58×10^9 K, which is lower than 3×10^9 K; explosive oxygen burning can occur if the temperature exceeds this value. This implies that the oxygen explosion cannot occur and the WD will eventually form an NS through AIC.

Figure 4 shows the density-temperature profiles of the ONe WD in the initial and final stages. At the onset of the accretion process, the surface of the WD is

compressed by the material, leading to the formation of a convection zone on the surface. The ^{12}C+^{12}C nuclear reactions are triggered when the ignition conditions of the carbon shell are satisfied, transforming the carbon into heavier elements (e.g., ^{20}Ne and ^{24}Mg). The ONe WD continuously grows in mass and eventually reaches $1.389\,M_{\odot}$. Note that there are two burning regions in the center of the core in the final stage. The burning zone for the relatively low density position ($\log\rho_{\rm c} \sim 9.6$) is caused by the electron-capture reactions of ^{24}Mg, whereas the innermost zone is caused by the electron-capture reactions of ^{20}Ne and oxygen burning, in which the central nuclear reaction rate exceeds $2.5 \times 10^{8}\,{\rm erg\,g^{-1}\,s^{-1}}$.

Figure 5 presents the elemental abundance distribution for the ONe WD in the final stage, which can provide initial input parameters when simulating the AIC processes. Nuclear fusion transforms the carbon into ^{20}Ne and ^{24}Mg after the flashes occur, resulting in higher abundances of neon and magnesium on the surface. In the center of the WD, the exothermal electron-capture reactions of ^{24}Mg generate a burning wave, which propagates outside the core and transforms all ^{24}Mg into ^{24}Ne in the center. The abundance of ^{20}O in the center increases sharply after the electron-capture reaction chain $^{20}{\rm Ne} \rightarrow {}^{20}{\rm F} \rightarrow {}^{20}{\rm O}$ is triggered. However, the temperature and density needed for electron-capture reaction of ^{20}F are much lower than those of ^{20}Ne, resulting in the ^{20}F being transformed into ^{20}O immediately once it appears (see Schwab et al. 2015).

3.2 Results of Different Initial WD Masses and Accretion Rates

In order to investigate whether the initial WD mass ($M^{\rm i}_{\rm WD}$) and accretion rate ($\dot{M}_{\rm acc}$) influence the final fate of accreting ONe WDs or not, we simulate the long-term evolution of accreting ONe WDs with different $M^{\rm i}_{\rm WD}$ and $\dot{M}_{\rm acc}$. The results are summarized in Table 1.

Figure 6 presents the central density-temperature evolutionary profiles for the different initial masses of accreting ONe WDs, in which $M^{\rm i}_{\rm WD}$=1.15, 1.2 and $1.3\,M_{\odot}$. In this simulation, $\dot{M}_{\rm acc} = 1.0{\times}10^{-5}\,M_{\odot}\,{\rm yr^{-1}}$. Although $\rho_{\rm c}$ and $T_{\rm c}$ are different at the onset of the simulations, they tend to be similar as the WDs increase in mass. The electron-capture reactions of ^{24}Mg and ^{20}Ne occur at the same temperature and density, and all of the WDs experience AIC at the end of the calculations. This implies that different initial WD masses have negligible influence on the final outcome of accreting ONe WDs. Note that a bifurcation appears at the end of the evolutionary track of $1.3\,M_{\odot}$ due to numerical reasons, which has no influence on the final outcome.

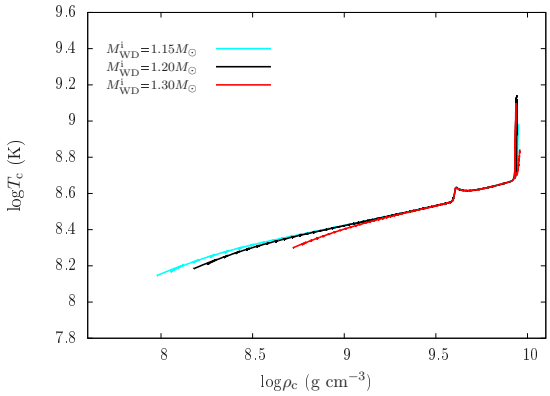

Fig. 6 Central density-temperature profiles for the evolution of accreting ONe WDs, in which $\dot{M}_{\rm acc} = 1.0 \times 10^{-5}\,M_{\odot}\,{\rm yr^{-1}}$.

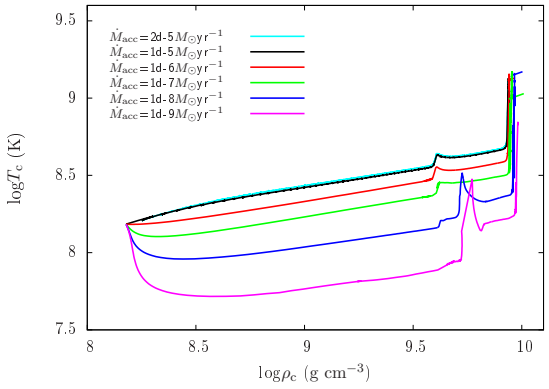

Fig. 7 Similar to Fig. 6, but for various accretion rates, in which $M^{\rm i}_{\rm WD} = 1.2\,M_{\odot}$.

The accretion rates may also influence the mass-accretion timescale and the corresponding evolution of $T_{\rm c}$. Here, we simulate the evolution of a $1.2\,M_{\odot}$ ONe WD with a wide range of $\dot{M}_{\rm acc}$. In Figure 7, we present the central density-temperature profiles of the accreting ONe WD with different $\dot{M}_{\rm acc}$. For low $\dot{M}_{\rm acc}$, $T_{\rm c}$ is lower due to longer evolution timescale of the accreting WDs. Note that $\dot{M}_{\rm acc}$ has little influence on $\rho_{\rm c}$ at the onset of electron-capture reactions of ^{20}Ne. However, the profiles are not similar to that of ^{24}Mg, especially in the cases of $\dot{M}_{\rm acc} = 1.0 \times 10^{-8}$ and $1.0 \times 10^{-9}\,M_{\odot}\,{\rm yr^{-1}}$. This is because, for lower $\dot{M}_{\rm acc}$, the electron-capture reaction $^{24}{\rm Mg} \rightarrow {}^{24}{\rm Na}$ occurs at a relatively lower temperature, but the electron-capture reaction of ^{24}Na is not trig-

Table 1 Parameters of Accreting ONe WDs with Different Initial Masses and Accretion Rates

$M^{\rm i}_{\rm WD}$ ($M_\odot$)	$\dot{M}_{\rm acc}$ ($M_\odot\,{\rm yr}^{-1}$)	$t_{\rm e}$ (yr)	$M^{\rm f}_{\rm WD}$ ($M_\odot$)	$\log R^{\rm f}_{\rm WD}$ ($R_\odot$)	$\log \rho^{\rm f}_{\rm c}$ (g cm^{-3})	$\log T^{\rm f}_{\rm c}$ (K)
1.20	2.0×10^{-5}	1.323×10^{4}	1.389	–2.532	9.9386	8.8892
1.15	1.0×10^{-5}	3.259×10^{4}	1.389	–2.624	9.9366	8.9943
1.20	1.0×10^{-5}	2.111×10^{4}	1.389	–2.572	9.9394	8.7058
1.30	1.0×10^{-5}	9.851×10^{3}	1.389	–2.633	9.9744	8.8057
1.20	1.0×10^{-6}	1.873×10^{5}	1.387	–2.683	9.9407	9.1180
1.20	1.0×10^{-7}	1.859×10^{6}	1.386	–2.707	9.9514	9.0288
1.20	1.0×10^{-8}	1.840×10^{7}	1.384	–2.708	9.9664	9.1528
1.20	1.0×10^{-9}	1.830×10^{8}	1.383	–2.714	9.9811	8.8240

Notes: $M^{\rm i}_{\rm WD}$ = initial WD mass; $\dot{M}_{\rm acc}$ = mass accretion rate; $t_{\rm e}$ = evolution time; $M^{\rm f}_{\rm WD}$ = final WD mass; $\log R^{\rm f}_{\rm WD}$ = final WD radius; $\log\rho^{\rm f}_{\rm c}$ = final central density of the WD; $\log T^{\rm f}_{\rm c}$ = final central temperature of the WD.

gered (see fig. 4 in Schwab et al. 2015). The conditions in the central zone will be satisfied with the reaction chain $^{24}{\rm Na}\rightarrow{}^{24}{\rm Ne}$ as $\rho_{\rm c}$ increases, leading to the subsequent increase of $T_{\rm c}$. Thus, the evolutionary tracks of density-temperature are different for $\dot{M}_{\rm acc}=1.0\times10^{-8}$ and $1.0\times10^{-9}\,M_\odot\,{\rm yr}^{-1}$.

In Figure 8, we present the elemental abundance distribution profiles in the final stage of a $1.2\,M_\odot$ ONe WD with three different accretion rates. Note that the elemental abundances of carbon in the shells are different from that of Figure 5. This is because, for low $\dot{M}_{\rm acc}$, the surface temperatures are lower due to longer evolution timescale, resulting in the carbon burning not occurring in the shell of the WDs. Meanwhile, for lower $\dot{M}_{\rm acc}$, the temperature of the core is cooler when the electron-capture reaction of $^{24}{\rm Mg}$ occurs. At the relatively low temperature, the electron-capture rate of $^{24}{\rm Mg}$ is higher than that of $^{24}{\rm Na}$. Thus, the elemental abundance of $^{24}{\rm Na}$ in the core becomes higher as $\dot{M}_{\rm acc}$ decreases. Similarly, the occurrence of electron-capture reactions of $^{20}{\rm Ne}$ needs higher $\rho_{\rm c}$ when the core is cooler (see fig. 4 in Schwab et al. 2015). This indicates that the core becomes denser for lower $\dot{M}_{\rm acc}$ when AIC occurs (see also Fig. 5). Thus, the final WD radiuses in Table 1 are smaller for lower $\dot{M}_{\rm acc}$.

4 DISCUSSION AND CONCLUSIONS

The WDs in a binary would merge together due to the loss of orbital angular momentum. However, the merger process is still under debate. Several studies suggested that a fast merger may occur if the mass ratio of two WDs is larger than 2/3, in which the WD binary would merge dynamically, resulting in a high mass-transfer rate (e.g., $10^4\,M_\odot\,{\rm yr}^{-1}$; see Zhang & Jeffery 2012). Yoon et al. (2007) indicated that not all of the material from the secondary transfers onto the primary WD to form a hot corona. In their model, the remaining material could form a Keplerian disc surrounding the primary WD, and the mass-transfer rate from the Keplerian disc may be less than $5.0\times10^{-6}\,M_\odot\,{\rm yr}^{-1}$. Note that the merger models still remain uncertain, especially when rotation is taken into account; Saio & Nomoto (2004) suggested that the accretion rates may decrease if the primary WD approaches a critical rotation. In our simulations, we only considered constant accretion rates to represent the thick disc model. Stable mass transfer would occur during the accretion, and the mass-accretion rate from the thick disc is usually less than $2.0\times10^{-5}\,M_\odot\,{\rm yr}^{-1}$. This indicates that our assumption is feasible.

The final outcomes of the ONe core have been investigated by some studies so far. However, they are still not understood completely. Since the ONe core contains nuclear fuel inside, the WD may undergo oxygen or neon deflagration when its mass approaches $M_{\rm Ch}$. Isern et al. (1991) found that a thermonuclear supernova may be produced if the ignition density of oxygen is lower than $9.5\times10^{9}\,{\rm g\,cm^{-3}}$. Recently, Jones et al. (2016) simulated the oxygen deflagration processes of a degenerate ONe core. Their results supported the 1D simulations of Isern et al. (1991), and also suggested that the ONe WD can collapse into an NS if the ignition density of oxygen is relatively high (e.g., $2\times10^{10}\,{\rm g\,cm^{-3}}$). In our simulations, we used temperature as the criterion for AIC, which means that the AIC can be triggered if $\log T_{\rm c}$ of the ONe WD during the final stage cannot exceed 9.6 (i.e., the temperature of explosive oxygen ignition). The temperature criterion is also supported by some studies (e.g., Schwab et al. 2015). Our simulations show that $T_{\rm c}$ cannot exceed 1.58×10^{9} K due to the neutrino-loss mechanism. This implies that $\rho_{\rm c}$ will increase until AIC occurs.

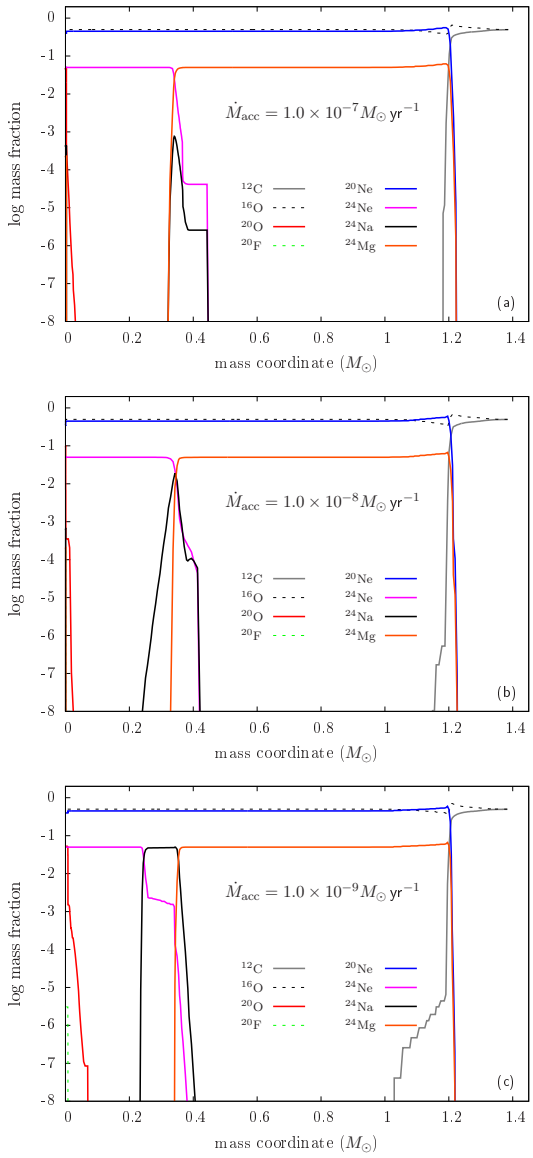

Fig. 8 Similar to Fig. 5, but for various accretion rates, in which $M^{\rm i}_{\rm WD} = 1.2\,M_\odot$. Panel (*a*): $\dot{M}_{\rm acc} = 1.0 \times 10^{-7}\,M_\odot\,{\rm yr}^{-1}$; Panel (*b*): $\dot{M}_{\rm acc} = 1.0 \times 10^{-8}\,M_\odot\,{\rm yr}^{-1}$; Panel (*c*): $\dot{M}_{\rm acc} = 1.0 \times 10^{-9}\,M_\odot\,{\rm yr}^{-1}$.

In our simulations, we set the initial $X_{\rm Mg}$ to be 5%. However, various $X_{\rm Mg}$ may influence the evolution of $T_{\rm c}$ and $\rho_{\rm c}$ when electron-capture reaction of ^{24}Mg is triggered. Schwab et al. (2015) explored the evolutions of an ONe core with a wide range of $X_{\rm Mg}$ (i.e., 0.01 – 0.2). In their studies, $T_{\rm c}$ and $\rho_{\rm c}$ of the ONe WDs have similar evolution tracks if $X_{\rm Mg} \leq 0.05$, but for higher $X_{\rm Mg}$ the electron-capture reaction of ^{20}Ne is triggered in a relatively high $\rho_{\rm c}$. This implies that $X_{\rm Mg}$ in the initial WDs may not affect the final outcome of ONe cores (i.e., collapse into an NS) when their masses approach $M_{\rm Ch}$ based on the results of Jones et al. (2016). Meanwhile, we have not considered the Urca-process cooling in our simulations, which may influence the evolution of an accreting ONe WD. However, Schwab et al. (2017) found that $\rho_{\rm c}$ of the ONe WD is a little bit larger than that without Urca-process cooling when oxygen is ignited, which means that the final outcome of ONe cores will not be changed.

Comparing with the standard core collapse channel, NSs originating from the AIC channel may have some special properties. (1) AIC may produce NSs with high magnetic fields and slow rotation rates if the AIC process occurs near the end of the mass transfer stage, which may explain the existence of NSs with high magnetic fields and slow rotation rates in close binary systems found in the Galactic disk (e.g., Yungelson et al. 2002; Tauris et al. 2013). (2) NSs from this channel generally receive a smaller kick than those from the standard core collapse channel, and the evolution time of progenitor systems for AIC is longer, which may explain the existence of young NSs living in globular clusters (e.g., Boyles et al. 2011; Tauris et al. 2013). (3) The mass donors of NSs from this channel may have ultra-low masses, since a large amount of material is transferred to the primaries during the binary evolution phases (e.g., Lyne et al. 1993).

By employing `MESA`, we investigated the long-term evolution of ONe WDs during the mass-accretion process. We adopted different initial WD masses (i.e., $M^{\rm i}_{\rm WD}$=1.15, 1.2 and 1.3 $M_\odot$) and accretion rates (i.e., $1.0 \times 10^{-9} \leq \dot{M}_{\rm acc} \leq 2.0 \times 10^{-5}\,M_\odot\,{\rm yr}^{-1}$) in our simulations. Our results indicate that $M^{\rm i}_{\rm WD}$ and $\dot{M}_{\rm acc}$ could affect the evolution of $T_{\rm c}$ and $\rho_{\rm c}$ associated with the WDs, but explosive oxygen ignition cannot be triggered by the exothermic process of electron-capture reactions. This implies that ONe WDs will finally undergo AIC to form NSs. Note that rotation may influence the structure of the accretion disc and the subsequent outcomes of the ONe WDs (e.g., Yoon et al. 2007). However, the current study on the influence of rotation still remains uncertain and needs to be investigated further. Finally, we hope that AIC events can be identified in the future, which will be useful for the studies of binary evolution and electron-capture supernovae.

Acknowledgements We acknowledge useful comments and suggestions from the referee. This study is supported by the National Basic Research Program of China (973 program, 2014CB845700), the Chinese Academy

of Sciences (Nos. KJZD-EW-M06-01 and QYZDB-SSW-SYS001), the National Natural Science Foundation of China (Nos. 11673059, 11521303, 11390374 and 11573016) and the Natural Science Foundation of Yunnan Province (Nos. 2013HB097, 2013HA005 and 2017HC018).

References

Abdikamalov, E. B., Ott, C. D., Rezzolla, L., et al. 2010, Phys. Rev. D, 81, 044012
Bailyn, C. D., & Grindlay, J. E. 1990, ApJ, 353, 159
Benz, W., Bowers, R. L., Cameron, A. G. W., & Press, W. H. . 1990, ApJ, 348, 647
Bhattacharya, D., & van den Heuvel, E. P. J. 1991, Phys. Rep., 203, 1
Boyles, J., Lorimer, D. R., Turk, P. J., et al. 2011, ApJ, 742, 51
Brooks, J., Bildsten, L., Schwab, J., & Paxton, B. 2016, ApJ, 821, 28
Brooks, J., Schwab, J., Bildsten, L., Quataert, E., & Paxton, B. 2017, ApJ, 843, 151
Dar, A., Kozlovsky, B. Z., Nussinov, S., & Ramaty, R. 1992, ApJ, 388, 164
Denissenkov, P. A., Herwig, F., Bildsten, L., & Paxton, B. 2013, ApJ, 762, 8
Fryer, C., Benz, W., Herant, M., & Colgate, S. A. 1999, ApJ, 516, 892
Hachisu, I., Kato, M., & Nomoto, K. 1996, ApJ, 470, L97
Han, Z., & Podsiadlowski, P. 2004, MNRAS, 350, 1301
Hartmann, D., Woosley, S. E., & El Eid, M. F. 1985, ApJ, 297, 837
Hurley, J. R., Tout, C. A., Wickramasinghe, D. T., Ferrario, L., & Kiel, P. D. 2010, MNRAS, 402, 1437
Isern, J., Canal, R., & Labay, J. 1991, ApJ, 372, L83
Itoh, N., Tomizawa, N., Tamamura, M., Wanajo, S., & Nozawa, S. 2002, ApJ, 579, 380
Jones, S., Röpke, F. K., Pakmor, R., et al. 2016, A&A, 593, A72
Langer, N., Deutschmann, A., Wellstein, S., & Höflich, P. 2000, A&A, 362, 1046
Li, X.-D., & van den Heuvel, E. P. J. 1997, A&A, 322, L9
Lyne, A. G., Biggs, J. D., Harrison, P. A., & Bailes, M. 1993, Nature, 361, 47
Lyutikov, M., & Toonen, S. 2017, arXiv:1709.02221
Marquardt, K. S., Sim, S. A., Ruiter, A. J., et al. 2015, A&A, 580, A118
Metzger, B. D., Thompson, T. A., & Quataert, E. 2008, ApJ, 676, 1130
Miyaji, S., Nomoto, K., Yokoi, K., & Sugimoto, D. 1980, PASJ, 32, 303
Mochkovitch, R., & Livio, M. 1990, A&A, 236, 378
Moriya, T. J. 2016, ApJ, 830, L38
Nomoto, K., & Iben, Jr., I. 1985, ApJ, 297, 531
Nomoto, K., & Kondo, Y. 1991, ApJ, 367, L19
Paxton, B., Bildsten, L., Dotter, A., et al. 2011, ApJS, 192, 3
Paxton, B., Cantiello, M., Arras, P., et al. 2013, ApJS, 208, 4
Paxton, B., Marchant, P., Schwab, J., et al. 2015, ApJS, 220, 15
Piro, A. L., & Kollmeier, J. A. 2016, ApJ, 826, 97
Podsiadlowski, P., Rappaport, S., & Pfahl, E. D. 2002, ApJ, 565, 1107
Potekhin, A. Y., Chabrier, G., & Rogers, F. J. 2009, Phys. Rev. E, 79, 016411
Qian, Y.-Z., & Wasserburg, G. J. 2007, Phys. Rep., 442, 237
Saio, H., & Jeffery, C. S. 2000, MNRAS, 313, 671
Saio, H., & Jeffery, C. S. 2002, MNRAS, 333, 121
Saio, H., & Nomoto, K. 2004, ApJ, 615, 444
Schwab, J., Quataert, E., & Bildsten, L. 2015, MNRAS, 453, 1910
Schwab, J., Quataert, E., & Kasen, D. 2016, MNRAS, 463, 3461
Schwab, J., Bildsten, L., & Quataert, E. 2017, MNRAS, 472, 3390
Takahashi, K., Yoshida, T., & Umeda, H. 2013, ApJ, 771, 28
Tauris, T. M., Sanyal, D., Yoon, S.-C., & Langer, N. 2013, A&A, 558, A39
Usov, V. V. 1992, Nature, 357, 472
Wang, B., Meng, X., Chen, X., & Han, Z. 2009, MNRAS, 395, 847
Wang, X., Wang, L., Filippenko, A. V., Zhang, T., & Zhao, X. 2013, Science, 340, 170
Wang, B., Li, Y., Ma, X., et al. 2015, A&A, 584, A37
Wang, B., Podsiadlowski, P., & Han, Z. 2017, MNRAS, 472, 1593
Wang, B. 2018, arXiv:1801.04031
Wu, C.-Y., Liu, D.-D., Zhou, W.-H., & Wang, B. 2016, RAA (Research in Astronomy and Astrophysics), 16, 160
Wu, C., Wang, B., Liu, D., & Han, Z. 2017, A&A, 604, A31
Yoon, S.-C., Podsiadlowski, P., & Rosswog, S. 2007, MNRAS, 380, 933
Yungelson, L. R., Nelemans, G., & van den Heuvel, E. P. J. 2002, A&A, 388, 546
Zhang, X., & Jeffery, C. S. 2012, MNRAS, 419, 452
Zhang, X., Jeffery, C. S., Chen, X., & Han, Z. 2014, MNRAS, 445, 660